Incubation and latency time estimation for SARS-CoV-2

Arntzen, V.H.

This chapter will be submitted soon as Vera H. Arntzen, Manh Nguyen Duc, Marta Fiocco, Lan Truong Thi Thanh, Tam Nguyen Hoai Thao, Buu Mai Thanh, Tu-Anh Nguyen, Nhat Le Thanh Hoang, Marc Choisy, Lam Phung Khanh, Nga Le Hong and Ronald B. Geskus, on behalf of the Covid-19 modelling team Oxford University Clinical Research Unit, Vietnam[+]. The latency time of the SARS-CoV-2 Delta variant in naive individuals from Vietnam.

[+] *Duc Du Hong, Lam Phung Khanh, Leigh Jones, Marc Choisy, Nhat Le Thanh Hoang, Ronald Geskus, Sonia Lewycka, Thomas Kesteman, Trinh Dong Huu Khanh, Tung Trinh Son, Manh Nguyen Duc, Nguyet Nguyen Thi Minh, Thinh Ong Phuc, Trang Duong Thuy, Lieu Tran Thi Bich, Maia Rabaa.*

The latency time of the SARS-CoV-2 Delta variant in naive individuals from Vietnam

Contents

Abstract

The latency time (infection to start-of-infectiousness) is one of the factors that determines the efforts required to control an infectious disease. Yet, estimates of the SARS-CoV-2 latency time remain sparse. Information on the endpoint requires repeated testing for viremia. Moreover, proper estimation is challenging as both the start- and endpoint are typically interval censored and long latency times may be underrepresented.

We collected detailed exposure information from public health reports produced during an outbreak with the SARS-CoV-2 Delta variant in Ho Chi Minh City, Vietnam, from May 2021 onwards. Using a tailor-made digital form and application to make reliable choices, we distilled a comprehensive data set with information on exposure and test results from 1951 individuals. This is the first data set of its kind outside of China, collected in the absence of large-scale vaccination or earlier transmission.

Our analysis is unique as we respect the doubly interval censored nature of the observations and make realistic assumptions regarding the infection risk (exponential growth) and the latency time distribution (generalized gamma), while also addressing truncation due to sampling cutoff and a finite quarantine length. Our implementation using the Bayesian program JAGS is freely available in the R package `doublIn`.

The estimated mean SARS-CoV-2 Delta variant's latency time was 3.22 (95% Credible Interval 2.89; 3.55) days; the median 1.81 (95% CrI 1.44; 2.16); the 95% percentile 10.98 (95% CrI 9.91; 12.41). Sensitivity analyses showed that the estimates depend strongly on the model assumptions.

Our results indicate that the SARS-CoV-2 Delta latency time may be shorter than previously assumed, requiring timely identification of infecteds. This may explain why the combination of contact tracing and quarantine was a more successful strategy for variants characterized by a longer latency time.

Keywords latency time □ SARS-CoV-2 □ contact tracing data □ doubly interval censoring □ quarantine

4.1 Introduction

Understanding the natural history of SARS-CoV-2 variants has been essential to shape public health measures optimally. Viral shedding patterns differ per SARS-CoV-2 variant [Puhach et al., 2023], and it naturally follows that the latency time (infection to start of infectiousness) is variant-specific as well. Quarantine length is one of the public health measures that is ideally informed by latency time. However, given the sparsity of such estimates, the choice of quarantine length is typically based on estimates of the incubation time (infection to symptom onset) distribution, even though 40.5% of the SARS-CoV-2 infected individuals do not develop symptoms [Ma et al., 2021]. Knowledge of the latency time is essential, as quarantining is cumbersome for individuals and demanding in terms of logistics, especially when performed in a designated facility, as was the policy in countries like Vietnam. More generally, estimates of the latency time indicate how extensive a public health response needs to be to control the spread of SARS-CoV-2 [Demers et al., 2023]. The shorter the latency time, the less time there is to identify and isolate new cases before they potentially transmit to others. Together with the basic reproduction number R_0 and the amount of non-symptomatic transmission, the latency time determines the required effort to control spread of an infectious disease.

Literature on the SARS-CoV-2 latency time distribution is scarce [Kang et al., 2022; Ma et al., 2022; Jiang et al., 2023; Xin, Li, Wu, Li, Lau, Qin, Wang, Cowling, Tsang and Li, 2021; Li et al., 2024]. As the roll-out of vaccination campaigns coincided with the emergence of novel variants, one cannot easily compare the estimates between variants. Current estimates of latency time are from China and concern either the Delta variant in the presence of partial vaccination [Kang et al., 2022; Ma et al., 2022; Li et al., 2024], or individuals of which both the vaccination status and the variant are unknown [Xin, Li, Wu, Li, Lau, Qin, Wang, Cowling, Tsang and Li, 2021]. Using a unique data set originating from Vietnam, we present the first estimate of the latency time of the SARS-CoV-2 Delta variant in mostly naive individuals.

Data to estimate latency time is difficult to collect, as both infection and start of infectiousness are not observed directly. Exposure information is typically collected by retrospectively interviewing notified cases as part of a contract tracing policy. When contact tracing is implemented such data is usually available, as we know from the availability of

estimates of the incubation time (infection to symptom onset). However, information about the endpoint of the latency time, i.e. the start of infectiousness, is rare. As we cannot observe the start of infectiousness, one typically chooses the start of RNA shedding as a proxy [Xin, Li, Wu, Li, Lau, Qin, Wang, Cowling, Tsang and Li, 2021; Kang et al., 2022; Li et al., 2024], which we refer to as start-of-shedding in this Chapter. When an individual tests positive by a PCR- or rapid antigen test, we assume that shedding has started. Hence, we assume that shedding started between the last negative test (when available) and the first positive test. Latency time can only be estimated if PCR- or antigen tests are performed repeatedly during follow-up. Since Vietnam adopted the policy of quarantining in facilities allocated by the government, PCR- and antigen tests were performed repeatedly during follow-up; therefore it is possible to estimate the latency time distribution using this data.

Observations of latency time are typically doubly interval censored, which means that both the start- and endpoint are at best known to fall in specific time windows. This complicates the analysis. To simplify estimation, common practice is to assume that the risk of infection within the exposure window is constant and that the latency time follows a gamma, lognormal or Weibull distribution. In previous work, we found that this can introduce bias in the estimates (Chapter 2). In this study, we relax these assumptions by considering alternative infection risk distributions using the observed trends in first positive test results in the population and using the more flexible generalized gamma distribution for the latency time, which includes the commonly used distributions as a special case. Also, we address right truncation to prevent sampling bias from two phenomena. First, longer latency times may be missed due to ongoing, increasing transmission during data collection [Chen et al., 2022; Xin, Li, Wu, Li, Lau, Qin, Wang, Cowling, Tsang and Li, 2021]. Second, as quarantine has a definite duration, some individuals may have started shedding afterwards. As far as we are aware, addressing the latter source of bias is a novelty in SARS-CoV-2 latency time estimation.

This paper is organized as follows. In Section 4.2, we provide a short overview about SARS-CoV-2 latency time estimates from the literature. In Section 4.3 information about data collection, extraction and cleaning is discussed. The methodology used and the results are presented in Sections 4.4 and 4.5 respectively. The article ends with a discussion where the implications of our findings and future directions of research are outlined.

4.2 Literature

Studies estimating the SARS-CoV-2 latency time are scarce. We found five studies that directly estimated the SARS-CoV-2 latency time, i.e. not inferring it from a model. Unfortunately, one paper by Jiang [Jiang et al., 2023], who is shared first author on one of the other papers [Li et al., 2024], was in Chinese and could not be accessed via our university.

All estimates of the SARS-CoV-2 latency time were based on contact tracing data from China, including repeated PCR-test results [Kang et al., 2022; Ma et al., 2022; Xin, Li, Wu, Li, Lau, Qin, Wang, Cowling, Tsang and Li, 2021; Jiang et al., 2023; Li et al., 2024].

The estimates concerned the Delta variant (n = 93 [Kang et al., 2022], n = 40 [Ma et al., 2022] and n = 672 [Li et al., 2024]), the Omicron variant (n = 467 [Jiang et al., 2023] and n = 885 [Li et al., 2024]) or unknown variant(s) (n = 177 [Xin, Li, Wu, Li, Lau, Qin, Wang, Cowling, Tsang and Li, 2021]). In two studies, the majority of the included individuals was vaccinated (70% [Ma et al., 2022], 57% for Delta and 92% for Omicron infected individuals [Li et al., 2024]) and in another at least part of the individuals was vaccinated [Kang et al., 2022]; for the other two studies vaccination status was unclear ([Xin, Li, Wu, Li, Lau, Qin, Wang, Cowling, Tsang and Li, 2021] [Jiang et al., 2023]). One study restricted the analysis to those with a single-day exposure [Ma et al., 2022], which simplifies analysis but may not be a representative selection [Li, Zhang, Peng, Gao, Jing, Wang, Ren, Xu and Wang, 2021].

4.3 Data

4.3.1 Spatiotemporal context

Because of its long-stretched border with China and limited ICU capacities, Vietnam initially strived to prevent any SARS-CoV-2 outbreak [Thai et al., 2020; Cobelens and Harris, 2020]. The country's public health response comprehended early and stringent policy measures, which included almost complete border closure, extensive contact tracing and quarantining. In 2020, the country experienced only one two-week period of national lockdown in April and a couple of local lockdowns. For an overview of the Vietnamese approach to the pandemic during its initial phase, we refer to Tan *et al.* [Tan, 2021].

Extensive contact tracing was employed, using an epidemiological classification system that is referred to as the 'F-system' [Hardy et al., 2020]. Direct (F_1) contacts and secondary (F_2) contacts (contacts of contacts) of confirmed cases (F_0) were actively traced. Contact tracing typically concerned the period from 14 to 21 days before testing positive or symptom onset of the confirmed case, whichever event occurred earlier, until the time of quarantine or the time of investigation. Contact tracing is bidirectional; it aims to find infection chains (infectees) from the F_0 onwards, but it also aims to find the source who infected the F_0. Attendance at events that are known to have led to transmission is explicitly asked for. For F_1 persons, besides finding possible (i.e. in case F_1 is infected) infectees (F_2), the public health staff also ask for the last date of exposure to the original case (F_0) to define the length of their quarantine. Direct contacts (F_1) as well as the rare incoming passengers that tested negative were required to quarantine in a government-allocated quarantine facility. Individuals were transferred to the hospital upon testing positive during quarantine. Secondary contacts (F_2) quarantined at home. Quarantine was for a minimum period of 14 days since the last date of exposure. For F_1 contacts and the incoming passengers it went up to three weeks from May 5^{th} to July 14^{th}, 2021 [Vietnam Center for Disease Control, 2021]. They ended their quarantine if they still tested negative at the end of this period. Once an F_1 tests positive, the person will be moved to the hospital, and all the contacts move from F_2 to F_1 status.

Until May 2021, Ho Chi Minh City in the south of Vietnam had barely reported any community transmission, because the few small-scale outbreaks were effectively contained. Community transmission considerably increased from mid May 2021 onwards. Infections were predominantly, and from June onwards solely, from the Delta variant, specifically the AY.57 lineage [Tam et al., 2023]. Vaccination campaigns still needed to be rolled out on a large scale. Before July 2021, Ho Chi Minh City received 923 050 vaccination doses [City Press Center Ho Chi Minh, 2021], on a city population of more than 10 million. In Vietnam in general, a populous country of 97.47 million, the daily number of administered vaccination doses only started to increase around June 14th, 2021, with total numbers increasing from 1.55 million to 4.06 million doses on July 12th [Our World in Data, 2024]. As such, we can assume that most individuals who were infected with SARS-CoV-2 during this period were naive, i.e. they did not contract SARS-CoV-2 before, and neither received vaccination. The Delta strain outbreak in Vietnam is thought to originate from a single

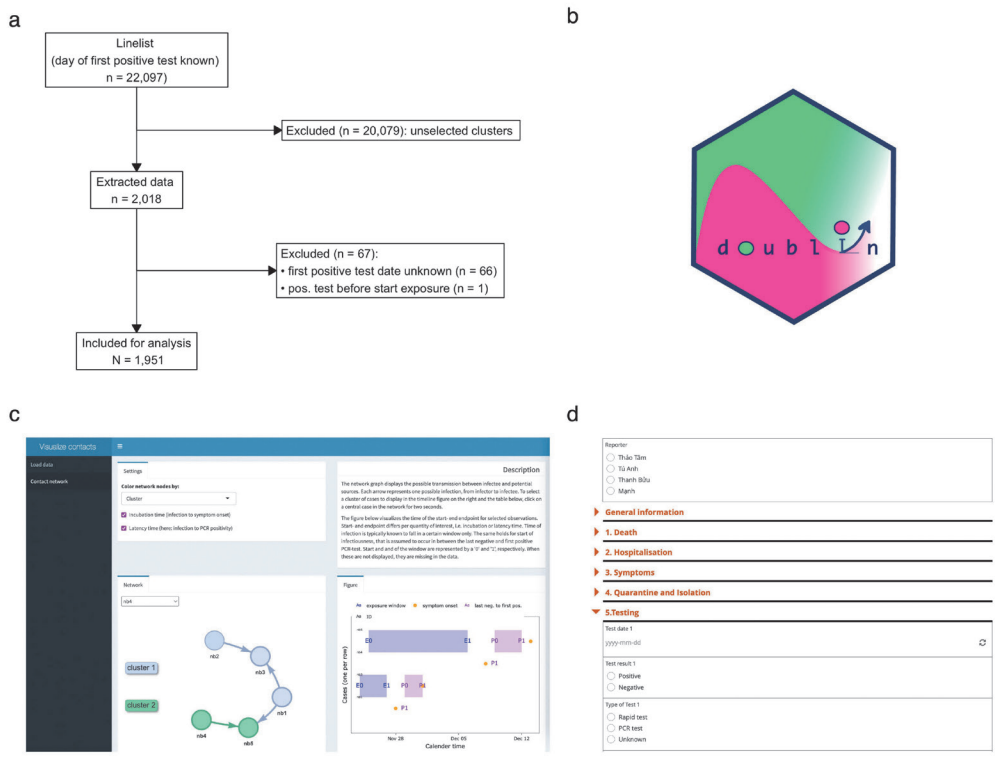

Figure 4.1: Illustration of the data collection process. Panel (**a**) shows the data flow from line list to data. Panel (**b**) shows the icon of the R package 'doublIn'. Panel (**c**) shows some of the R Shiny app functionalities (example data). Panel (**d**) shows the Kobo toolbox form used for data entry.

introduction in the second half of April 2021 [Tam et al., 2023].

The 2021 Ho Chi Minh City outbreak provides a rich data set that allows us to estimate the latency time of individuals for the Delta variant, as detailed exposure information and repeated test results are available. The line listing (data frame with one individual case per row) covers nearly all of the infections in this geographical region. The data used for analysis is representative of the population regarding the latency time due to the cluster-based sampling from the line listing, similar to snowball-sampling.

4.3.2 Data flow

Data in this study originates from several documents, provided by the Ho Chi Minh City Center for Disease Control (HCDC), which is the public health institute in Ho Chi Minh City. Flowchart 4.1a gives an overview. The starting point was a line list provided by HCDC containing basic information on 22097 PCR-confirmed cases, collected in Ho Chi Minh City between April 29th and July 15th, 2021. These collection dates refer to the day on which the case was made public; with the exception of one individual (excluded) the first positive test of any type (PCR or rapid antigen) always occurred before publication of the case, and typically three days before (34.2% of the individuals, n = 7576). The exact day of infection was generally unknown. Additional case information was retrieved from public health reports compiled as part of the contact tracing policy. We used 2827 public health reports in MS Word files. Each report covered one or multiple PCR-confirmed cases and gave more detailed information about exposure to potential sources. This information was obtained from individual case questionnaires that were taken upon confirmation of infection. We received the files in different folders, mostly but not exclusively covering a specific cluster of transmission. For simplicity, in the remainder of this paper we refer to 'cluster' as cases that were in the same folder. In July 2021, as the city saw a dramatic increase in the number of new cases, the contact tracing system got overwhelmed, and as a consequence not all cases could be described (timely) in public health reports.

4.3.3 Data extraction

During four months (from June 20th, 2022 to October 20th, 2022), four researchers (three from HCDC, one from the Oxford University Clinical Research Unit (OUCRU)) extracted the relevant case information. The researchers used a list with all clusters to divide their work. If a researcher found a link between the respective cluster and another cluster, the researcher would work on the related cluster next. For training purposes, at the very beginning, all four researchers worked on the same cluster of roughly 80 individuals. Then, they discussed their findings and aligned the way they retrieved data. Afterwards, the researchers started working independently, while the coordinating researcher from OUCRU performed random cross-checks of the data retrieved by the other researchers in the early stage of their work, again to align their work further. We included 75 of more than 100

clusters described by the public health reports in our data.

To support the data extraction from the public health reports, we developed a simple KoboToolbox form [KoBoToolbox, 2022] that facilitated manual data entry and prevented typos as much as possible. When a researcher read a report, they filled the relevant information into the form for those individuals that satisfied the following criteria: at least one potential source was mentioned in the report or at least one of two dates, namely the test date (PCR- or antigen test) or a day of onset of any symptom. When working on one cluster, the researcher typically drew all the potential transmission trees on paper, to assist with choosing the exposure periods.

If there was uncertainty in exposure, we considered two assumption in case one led to a narrower window than another. For instance, consider cases A and B residing together. They were exposed to a possible source between t_1 and t_2 and separated from each other at a later time t_3. Assuming that A and B contracted the infection from the same source led to the narrower window of t_1 to t_2. In the broader time frame of t_1 to t_3, we considered the possibility that A was initially infected from the source and subsequently transmitted the infection to B or vice versa.

To check and support the choice of these exposure windows, we developed an R Shiny application that visualizes the contact network based on entered data and the individual exposure information. We utilized the `KoboconnectR` R package [Sen, 2023] to directly import data collected from KoboToolbox that contained one row per infectee into R, facilitating visualization within our application.

Lastly, for the included cases, we merged the data obtained using KoboToolbox with the respective information of the initial line list, which had more complete information on testing.

Figure 4.1c and d give a glimpse of the KoboToolbox form and the Shiny app, respectively. The KoboToolbox form (Figure 4.1d) is available via `https://ee.kobotoolbox.org/x/dcXRd59G`. It supports entry of all relevant information from the public health reports, such as risk contacts and test results. Drop-down menus reduce the risk of data entry errors. We used the Shiny app (Figure 4.1c) to check if the extracted data was realistic. The software for both tools is available, with guidance and example data via `https://github.com/manhnguy/Contact-Tracing-for-Respiratory-Transmitted-Diseases`.

4.3.4 Cleaning

Our software suits observations for whom a) start of both windows (exposure and start-of-shedding) are known; b) both window widths (end minus start) are positive and non-zero; c) exposure coincides with, or occurs before the end of the start-of-shedding window.

For the vast majority (N = 2797, 94.8%) of all SARS-CoV-2 tests (N = 2950) performed during our study period on individuals in the extracted data (N = 2018, Figure 4.4b), the type of test was unknown, i.e. either a PCR or a rapid antigen test. We defined the first positive test date as the first day an individual tested positive for SARS-CoV-2 on *either* test. The last negative test date was defined as the day of the previous test of *either* type. For all individuals, the SARS-CoV-2 infection was confirmed by PCR test at some point during follow-up. We selected (Figure 4.1a) those observations for whom we had a positive test day, as well as at least one of the exposure window limits. For 1968 individuals out of 2018 for whom data was extracted, at least one test result was observed (Figure 4.4b). For 1952 individuals, the first positive test date was known (Figure 4.1a). We excluded one case for which the first positive test occurred before any exposure window (type 1 or 2) started. Hence, we included 1951 for analysis.

To comply with the requirements a-c, we prepared the data for analysis in six steps. We strived to include all possible information carried by the observations. We took the following steps in chronological order:

(i) if the end of exposure (E_r) is missing, set it to the day of the first positive test;

(ii) if the start of exposure (E_l) is missing, set it to the probable start of the Delta outbreak (April 30, 2021)

(iii) if the last negative test date (S_l) is missing, set it to the start of the exposure window ($S_l \leftarrow E_l$);

(iv) guarantee doubly interval-censored observations by considering a window width of at least one day in case date of infection or start-of-shedding were known, by adding or extracting half a day, respectively ($E_l - 0.5; E_r + 0.5; S_l - 0.5; S_r + 0.5$);

(v) if the exposure window ends after first positive test ($E_r > S_r$), let the end of exposure equal the first positive test date ($E_r \leftarrow S_r$);

(vi) if the last negative test occurs before start of exposure ($S_l < E_l$), set the last negative test to the start of exposure ($S_l \leftarrow E_l$).

Steps (i) to (vi) provided the subset of observations for analysis. Regarding step (v), note that we can naturally assume the individual to be infected by that time. We applied these rules separately for the two different ways exposure windows were determined.

4.4 Methods

4.4.1 Likelihood for doubly interval censored observations

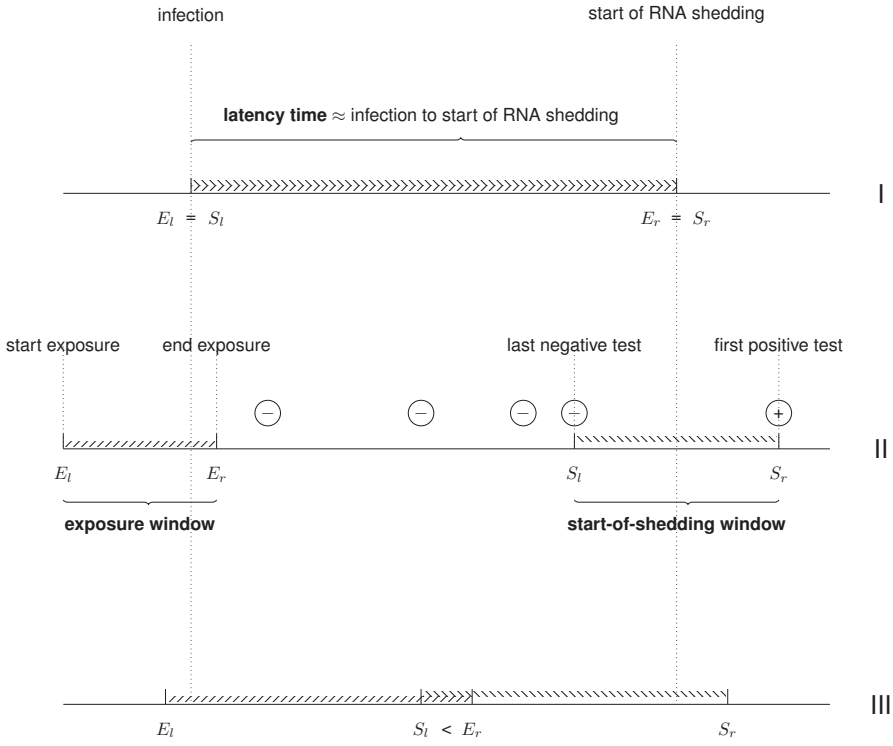

Figure 4.2: Illustration of observations of the latency time. Data representation of three individuals with an equal latency time which are observed differently due to double interval censoring. The window containing the origin is referred to as the exposure window, from the first possible moment of infection (E_l) to the last one (E_r). The boundaries of the window in which RNA shedding starts are the last negative test result and the first positive test result, where 'positive' refers to the detected presence of SARS-CoV-2 RNA (or antigen). The exposure window and start-of-shedding window may completely overlap ($E_l = S_I$ and $E_r = S_r$, indicated by I), not overlap ($E_r < S_l$, indicated by II) or partially overlap ($E_r > S_l$, indicated by III).

Building on previous work [Ramjith et al., 2022; Reich et al., 2009], the data representation of an observation of latency time consists of an exposure window and a start-of-shedding window that may completely coincide (I), not overlap (II), or partially overlap (III), as shown in Figure 4.2.

We first assume the setting without truncation. For an infected individual i $(i = 1, ..., N)$, let E_{il} and E_{ir} be the boundaries of the exposure window in calendar time; likewise, let S_l and S_r denote the start-of-shedding window.

Assume that the distributions of calendar time of infection (E) and latency time (E to S) are independent. When the exposure window ends before or on the same day as the start-of-shedding window begins (i.e. no overlap, Figure 1, type II), the contribution to the likelihood of the latency time for individual i is

$$l^{II} = \int_{e_{il}}^{e_{ir}} \int_{s_{il}}^{s_{ir}} g(e|e_{il}, e_{ir}) f(s-e) ds de \tag{4.1}$$

where $g(e|e_{il}, e_{ir})$ and $f(s-e)$ denote the probability density function of infection given the exposure window and the latency time respectively.

The likelihood contribution for an observation with complete overlap of the exposure and start-of-shedding windows (Figure 4.2, type I) is

$$l^{I} = \int_{e=e_{il}}^{e_{ir}} \int_{s=e}^{e_{ir}} g(e|e_{il}, e_{ir}) f(s-e) de ds. \tag{4.2}$$

When both windows partially overlap (i.e. Figure 4.2, type III) the likelihood $l(e_{il} \leq s_{il} \leq e_{ir} \leq s_{ir}$ can be decomposed in three parts using Equations 4.2 and 4.1. For details, we refer to the figure in Supplement 4.7.5.

4.4.2 Infection risk within the exposure window

The distribution of $g(e|e_{il}, e_{ir})$ depends on the assumptions made for the risk of infection within the exposure window $[e_l, e_r]$. A typical choice is a uniform distribution $g(e|e_{il}, e_{ir}) \sim Unif(e_{il}, e_{ir})$, implying that the infection risk is constant over time. However, the start of an outbreak is characterised by exponential growth and in previous work [Arntzen et al., 2023], we showed that violation of this assumption leads to biased estimates. Therefore, besides a constant risk, we explore an alternative assumption.

We assume an exponential growth for the infection risk at the population level. The incidence of new infections i is assumed to grow as $i(t) = i(t_0)e^{rt}$ where $i(t_0)$ is the

incidence when one started counting cases from the outbreak ($t = t_0$) and r is the epidemic growth rate (per day) with a corresponding doubling time of $\frac{ln(2)}{r}$ [Dorigatti et al., 2020]).

Estimates of growth rate and doubling time are obtained using the `R` package`incidence` [Kamvar et al., 2019]. We log-regressed the case incidence per day ($log[i(t)] = rt + log[i(t_0)]$) where we excluded all days on which the incidence was underreported (from July 12th onwards) to obtain the epidemic growth rate and doubling time, and corresponding Standard Error (SE). In the analysis we assume a normally distributed exponential growth factor with mean r and variance SE^2. Following Xin *et al.* [2021], we performed sensitivity analyses where we consider a less and more extreme scenario by extracting and adding $\approx$ 2 SEs to the estimated r, respectively. For the above-described approach, we assume that few infections will be unobserved in the line list, given the extensiveness of contact tracing.

4.4.3 Flexible distribution of latency time

The common practice in the literature is to fit three parametric distributions (gamma, lognormal and Weibull) and select one model by AIC (frequentist paradigm) or LOO IC (Bayesian paradigm). Especially when the interest is in the right-hand tail of the distribution, relaxing this assumption is recommended (Chapter 2). As the latency time may inform quarantine length, for which one often looks at estimates of the upper percentiles, we additionally fitted a generalized gamma distribution, first introduced by Stacy and Mihram [1965]; gamma, lognormal and Weibull distribution are special cases. For details on the parameterisation, we refer to Supplement 4.7.1. To implement the generalized gamma distribution, we used the parameterisation as proposed by Stacy and Mihram. As far as we know, there is only one earlier study on incubation and latency time estimation that utilized a generalized gamma distribution [Olivera and Muñoz, 2024].

4.4.4 Truncation

Our interest is to estimate the intrinsic latency time distribution [Park et al., 2024], which is representative for all individuals under stable conditions. However, due to several factors the likelihood (Eq. 4.2-4.3) does not directly concern the intrinsic distribution of interest in our data. Specifically, (i) the repeated testing for SARS-CoV-2 infection typically ended upon discharge from quarantine; (ii) cases that were made public after July 15th were not included in the line list from HCDC. Therefore, individuals for whom more time

elapsed between infection and first positive test are more likely to go unnoticed in our data than those for whom this interval is short, which is referred to as right truncation. If this phenomenon is not properly addressed, the latency time distribution is biased downwards in the early phase of an outbreak, which is illustrated with real data by Xin *et al.* [2021] and Chen *et al.* [2022]. Note that the size of the bias induced by (ii) is enlarged as the infection risk increased during the study period. We first discuss this issue in more detail, and then present how we addressed it in our analysis.

Individuals that kept on testing negative were typically dismissed from the quarantine facility after 21 days. Hence, there is a chance that individuals who have an exceptionally long latent period and would test positive for SARS-CoV-2 infection after quarantine have been missed. Figure 4.3a illustrates this phenomenon.

The cut-off criterion utilized by HCDC for the line list we obtained was that the publication date of a case was July 15th or earlier. Note that the first positive test typically occurred three days before publication. Therefore, individuals that were infected close to July 12th are less likely to be included in the data when they have a longer latency time (Figure 4.3b).

Xin *et al.* and Linton *et al.* addressed right truncation due to exponential growth or decay during the sampling phase in their analyses [Xin, Wong, Murphy, Yeung, Ali, Wu and Cowling, 2021; Linton et al., 2020] using their estimated exponential growth or decay factor r. This was formalized by Park *et al.* [2024] (see Eq. 23 in their paper). A difference between the likelihood proposed by Park which was utilized by Xin, and the approach by Linton is that the latter assumes a constant risk of infection within the exposure window, while addressing truncation due to exponential growth whereas Park and Xin assume an increasing risk within the exposure window.

For the truncation date for each individual $t_{i,end}$ in calendar time, we used the start of quarantine plus 21 days or July 12th (end of sampling), whichever occurred earlier in time. The start of quarantine was known for 53% of the included individuals (n = 1038); for the other half of the observations, July 12th was used as a truncation date. For those with unobserved quarantine date (43.8%, n = 913), the exposure window ends at first positive test or symptom onset, typically yielding wide exposure windows. Hence, these observations do not contribute much to the estimate.

Denote by $t_{i,end}$ the calendar time at which the observation was truncated; let the condition for the inclusion of individual i in the data set be $s_{ir} \leq t_{i,end}$, i.e. an individual

tests positive before the end of study. Recall that each individual observation of latency time $(e_{il}, e_{ir}, s_{il}, s_{ir})$ represents two coinciding (type I, Eq. 4.2), distinct (type II, Eq. 4.1) or partially overlapping (type III, Supplement 4.7.5) windows and therefore belongs to one of the three respective partitions of the data denoted by I, II or III (Figure 4.2). The likelihood of the complete set of observations $i = 1, ..., N$ addressing right truncation is

$$\prod_{i=1}^{N} \frac{l^I \cdot l^{II} \cdot l^{III}}{\int_{e_{il}}^{e_{ir}} g(e|e_{il}, e_{ir}) F(t_{i,end} - e) de}. \tag{4.3}$$

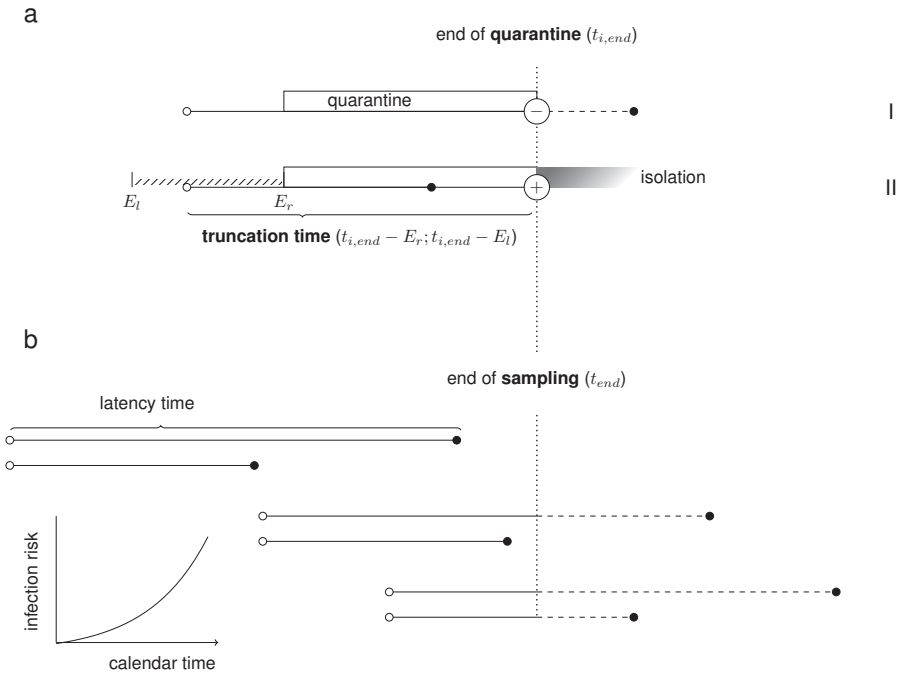

Figure 4.3: Illustration of truncation in the context of latency time estimation. Data representation of two individuals with a latency time of 9 days (upper) and 5 days (lower). In panel (**a**) both individuals were infected (open bullet) on the same calendar day and entered quarantine on the same day. However, individual I is unobserved (left quarantine while testing negative) whereas individual II tested positive by the end of quarantine and therefore appears in the data set with a (calendar) truncation time. Because infection is not observed exactly but known to fall within the exposure window $(E_l; E_r)$, the truncation time is interval censored. Panel (**b**) visualizes the same pair or latency times as before, but with different infection moment for each pair. Towards the end of the sampling period, relatively more individuals get infected due to exponential growth. The effect of truncation is the same as before.

4.4.5 Software

We used a Bayesian approach for estimation, using Markov Chain Monte Carlo to quantify the posterior distribution (Supplement 4.7.4). We extended code by Charniga *et al.*, used to estimate the incubation time for mpox [Charniga et al., 2022]. We adapted their code to allow for doubly interval censored data with all three types of observations of the latency time (example I, II and III in Figure 4.2). Apart from a constant infection risk within the exposure window we also considered exponential growth. For the latency time distribution we assumed gamma, Weibull and the more flexible generalized gamma model. We additionally corrected for right truncation (see Equation 4.3). The JAGS code that implements doubly interval censoring and right truncation is surprisingly concise as the different components can be combined without necessity to write down the complete likelihood (Supplement 4.7.4 for details). We assumed non-negative, flat priors for all parameters (normal distribution with μ = 0 and $\sigma^2 = 1000$, truncated at 0). We assumed that the uncertainty in the estimated epidemic growth rate r is normally distributed, with a standard deviation equal to the Standard Error of the estimate. We used the following settings: 3 chains, each with 500 000 iterations; a burn-in period of 10 000 and thinning factor 10, respectively.

We validated our code against the `coarseDataTools` package using simulated data, using Weibull and gamma for the time-to-event distribution, uniform distribution for infection and no right truncation. We found that the estimates were very similar (results not shown).

All analyses were performed in `R` Studio [RStudio Team, 2021]. Models were fitted via the `rjags` interface to JAGS [Plummer, 2017]. We used the ALICE computing resources provided by Leiden University. All code is available via *github.com/vharntzen/LatencyCovid Vietnam*.

4.4.6 Estimates

We report estimates of the mean, median, and the 95^{th} percentile, along with the corresponding 95% credible intervals. Parameter estimates that characterize the distributions can be found in Supplement 4.7.2.

Sensitivity analyses were performed in which only observations with narrow (≤ 4 days) exposure windows were analysed and in which truncation was not addressed

(Supplement 4.7.3).

4.5 Results

4.5.1 Descriptives

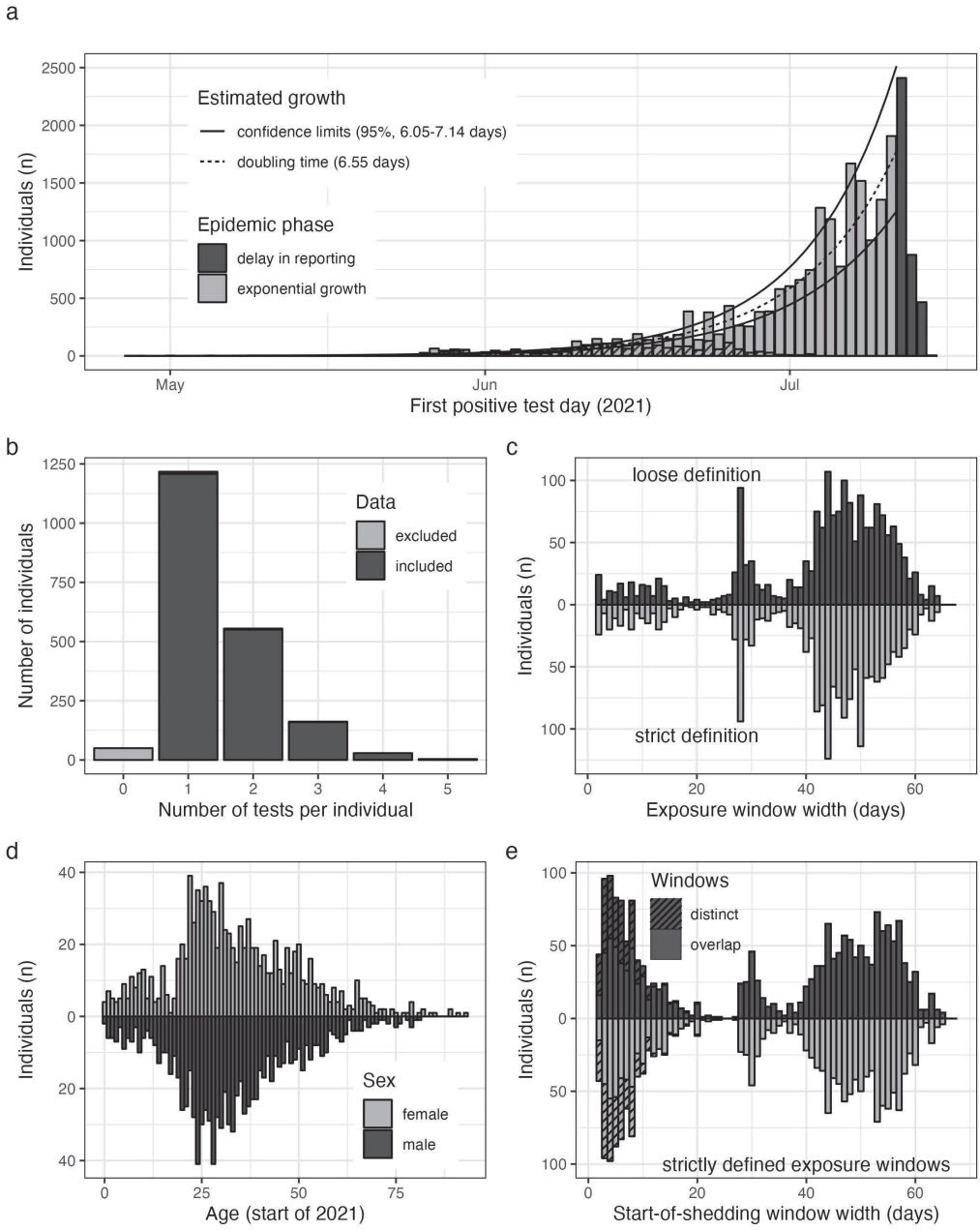

Figure 4.4: (Caption next page.)

Figure 4.4: Data characteristics. Panel (**a**): daily number of individuals from the line list that test positive for SARS-CoV-2 for the first time (per day on which the sample was taken). Greyscale indicates whether the data was used for estimation of the exponential growth factor (light grey) or considered underreporting (dark grey); the dashed part of each bar represents individuals included for analysis. As a first positive test typically occurred three days before a case was made public and the line list concerned all infecteds with publication on July 15th latest, the delay phase starts on July 12th, 2021. The solid line represents the estimated exponential growth curve; the dotted lines represent the confidence bounds around this curve. Panel (**b**): distribution of the total number of tests per individual. Note that the figure displays 2018 individuals for whom data was extracted. Only individuals with at least one test result (positive/negative) and known test day were included for analysis. Panel (**c**): the empirical distribution of the width of exposure windows included for analysis, according to a strict definition (below zero) and more loose definition (above zero). Panel (**d**): age distribution by sex of individuals included for analysis. Panel (**e**): the empirical distribution of start-of-shedding windows using different definitions of the exposure window (see above). Dashed areas indicate observations for whom exposure and start-of-shedding windows (partially) overlap.

Figure 4.4a visualizes the calendar day of first positive test of all individuals in the line list (N = 22,097). Excluding 3759 individuals (17.0%) with a first positive test for which the sample was taken from July 12th onwards (dark grey area) due to reporting delay as the public health system started to experience an overload, we estimated a doubling time of 6.55 days (95% CI 6.05; 7.14) with a corresponding exponential growth factor r of 0.106 (95% CI 0.097; 0.114).

The age distributions of males and females were almost equal (Figure 4.4d).

Figure 4.4c and e visualize the exposure window and start-of-shedding window widths, respectively, obtained by handling a more strict definition (below zero) and a looser definition (above zero) of the exposure window. Around 12% (n = 235) of individuals had an exposure window smaller than ten days (strict definition). The more strict definition did not decrease window widths substantially. The wider the start-of-shedding window, the more likely it is to overlap with the exposure window (Figure 4.4e). The start-of-shedding windows tend to be narrower than the exposure windows.

4.5.2 Estimates

Figure 4.5 visualizes the latency time estimates in our analyses and in the literature.

With the most flexible model (generalized gamma distribution), assuming exponential growth as estimated using the line list (r = 0.106), a strict assumption regarding the exposure window bounds, and addressing truncation, we estimated the latency time for the SARS-CoV-2 Delta variant as follows: mean 3.22 (95% CrI 2.89; 3.55) days; median 1.81 (95% CrI 1.44; 2.16); 95% percentile 10.98 (95% CrI 9.91; 12.41) (Figure 4.5a, dotted line and Figure 4.6).

Most outstanding is that all estimates are considerably larger when a constant infection risk is assumed instead of exponential growth (Figure 4.5a). The weaker and stronger exponential growth scenarios (r $\pm \approx$ 2SE) were comparable to the results assuming the estimated growth factor. The estimates when we considered a loose definition of the exposure window (Figure 4.5a, second row) are slightly smaller compared to the estimates using the strict definition. The differences between assuming generalized gamma, gamma and Weibull distributions were negligible.

The results of the sensitivity analyses are shown in Supplement 4.7.3. The impact of restricting the analysis to observations with a narrow (≤ 4 days) exposure windows was different per assumption for the infection risk. Assuming exponential growth, the estimates were larger, while for an assumed constant risk of infection these were smaller. Not addressing truncation shrunk the credible intervals, specifically obtaining more symmetric credible intervals around the 95^{th} percentile. When exponential growth was assumed, addressing truncation did not change the point estimates much; under the constant risk assumption the point estimates became larger.

4.6 Discussion

The Vietnamese data set of latency time observations is unique in its size and level of detail. Nonetheless, our estimates of the latency time distribution depend strongly on the assumptions that we made, specifically regarding the exposure window and the risk of infection within this window. We estimated a mean latency time of 3.22 (95% CrI 2.89; 3.55) days for mostly unvaccinated individuals predominantly infected with the Delta variant, with a median of 1.81 (95% CrI 1.44; 2.16) and a 95% percentile of 10.98

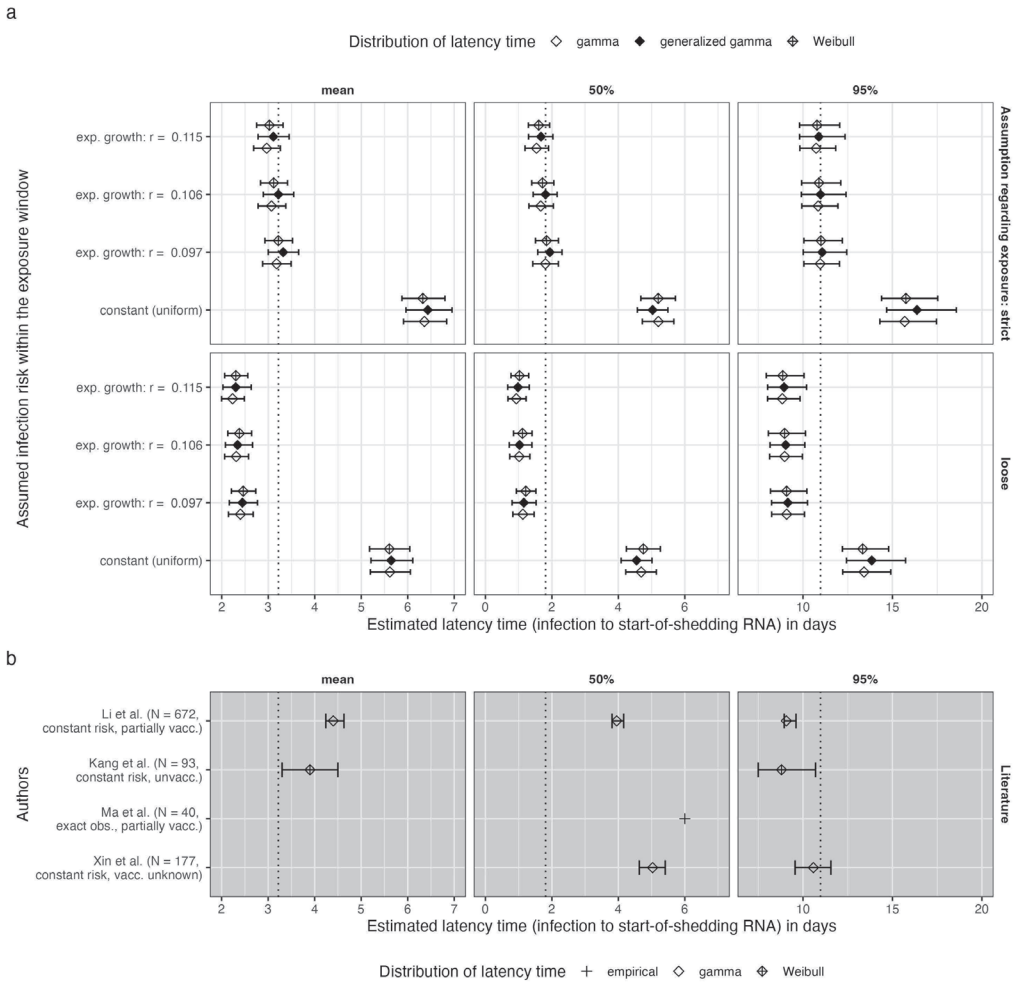

Figure 4.5: Latency time estimates for SARS-CoV-2. Panel (**a**): estimates based on our data concerning mostly the Delta variant; panel (**b**): estimates from the literature, concerning different variants. The mean, median and 95% percentile are presented with corresponding 95% credible intervals (**a**) or credible/confidence intervals (**b**) represented by error bars. Symbols refer to the assumed parametric shape of the distribution of latency time. All estimates are given in days (x-axis). In panel (**a**), estimates are given for different assumptions for the infection risk within the exposure window (y-axis) and exposure window definitions (rows). The estimated exponential growth rate was 0.106, with a standard error (SE) of 0.004; the results are shown assuming the estimated mean plus or minus 2 SEs as well.

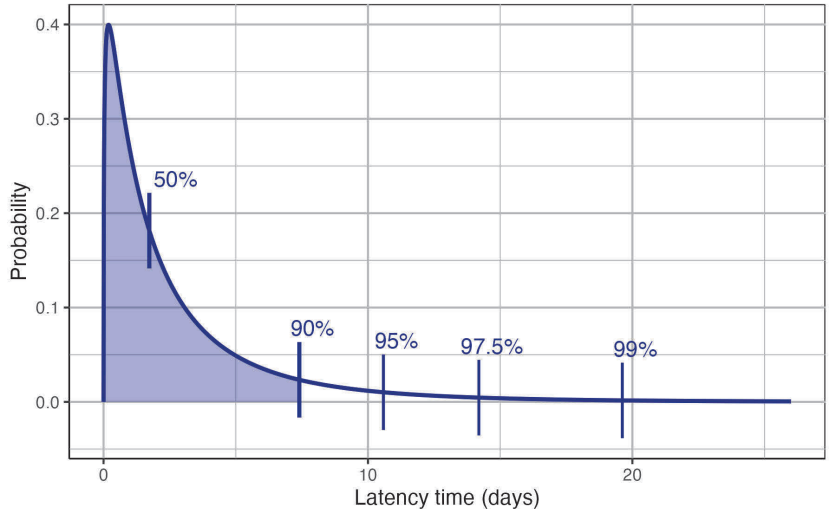

Figure 4.6: Estimated latency time distribution for SARS-CoV-2. Vertical bars correspond to the 50%, 90%, 95%, 97.5% and 99% percentile, respectively.

(95% CrI 9.91; 12.41) with the strict definition of the exposure window bounds. Our estimates assuming exponential growth are smaller than any of the estimates we found in the literature regarding the Delta variant.

As far as we are aware, we present the first estimate of the SARS-CoV-2 latency time for which the infection risk is assumed to increase according to the exponential growth of the case incidence. In similar analyses in the literature, it was assumed to remain constant in calendar time, which is known to be unrealistic during infectious disease outbreaks. Our analyses assuming a constant risk of infection provide estimates that are indeed comparable with most estimates in earlier studies (Figure 4.5b). However, it is unclear whether (part of) their observations concern the Delta variant. The estimates by Kang *et al.* for the Delta variant, assuming a constant risk, are considerably smaller than our estimates under the same assumption [Kang et al., 2022]. This is especially surprising given that they estimated a larger exponential growth rate during their sampling phase (0.33, 95% CrI: 0.18–0.48) than we found using our data (0.106, 95% CI 0.097; 0.114). In contrast to our analyses and the analysis by Xin *et al.* [2021], none of the other papers on SARS-CoV-2 latency time mentioned that they address truncation in their analysis.

Incubation time and latency time are closely related. In a large study, the mean

incubation time for the Delta variant was estimated to be 4.43 days (95% CI 4.36 – 4.49) [Galmiche et al., 2023]. Unfortunately, we could not estimate the incubation time distribution because our data on symptom onset was incomplete. Our estimate of the latency time is shorter, as one would expect given the possibility of presymptomatic spread of the infection [Tindale et al., 2020]. As Galmiche *et al.* noted, comparing the incubation time for variants is complicated due to differences in study design and vaccination status, and the same holds for latency time estimates.

We can safely assume that the vast majority of infections concerns the Delta variant and was unvaccinated at the time of infection. Note that the Vietnamese population is relatively young, e.g. median age is 31 (IQR 23; 43) in our data set and 31.6 countrywide (2020 [United Nations, Department of Economic and Social Affairs, Population Division, 2022]). Our estimate of the latency time distribution is probably generalizable to other low- and middle income countries with a similar age structure. Our study contributes by providing ready-to-use software that extends the current methods by addressing right truncation as we discussed before as well as in two other aspects that we discuss next.

We modelled the infection risk within the exposure window assuming exponential growth. The exponential growth factor r that we used in our analyses was based on the simple relationship where the incidence $i(t)$ can be expressed as $i(t) = i(t_0)e^{rt}$ where t_0 is the start of an outbreak. Note that the exponential growth factor (r) determines the doubling time ($ln(2)/r$) of an infectious disease. One caveat is that strictly speaking t_0 is unknown [Anzai and Nishiura, 2022]. The alternative equation proposed by Anzai *et al.* uses the time elapsed since one started counting cases from the outbreak (t_0), denoted by τ, i.e. $i(t) = i(t_0)e^{rt} \cdot \frac{e^{r\tau}-e^{-r}}{r}$. However, as there was basically no transmission in Vietnam just before the Delta outbreak started, we assumed that $\tau \approx 0$. Another limitation is that for some individuals, the population risk does not equal the individual risk within their exposure window, for example, when an infection is introduced into a household (Chapter 2). When viral sequencing data is available, one can obtain more certainty in the pairing of infector and infectee using the method described by Stockdale *et al.* [2023]. This would yield narrower exposure windows and thus milder bias when there is a discrepancy between the true and assumed infection risk distribution.

We contribute to the literature in the field by providing our code for doubly interval censored observations, which allows to assume an exponentially increasing (or decreasing)

risk within the exposure window, various assumptions regarding the shape of the latency time distribution and to address right truncation, implemented using JAGS [Plummer, 2017]. As WHO stressed after the emergence of SARS-CoV-1 [WHO, 2003], coronaviruses tend to have a long tailed incubation time distribution. In earlier work, we found that the common choices of parametric distributions (gamma, lognormal, Weibull) do not always capture the shape of the tail adequately, which is particularly problematic as the tail of the distribution informs quarantine length. Moreover, with parametric choices that differ by study, pooling estimates is not easy [McAloon et al., 2020]. Therefore, we assumed a generalized gamma distribution to allow for more flexibility regarding the shape of the latency time distribution. In the future, it would be worth exploring even more flexible methods such as splines that allow for simultaneous estimation of infection and latency time. The `R` package `TwoTimeScales` currently only includes exact and right censored observations; however the authors plan to extend this [Carollo et al., 2023].

One can also use our software for incubation time estimation as the symptom onset is typically interval censored with a window of one day. Furthermore, it can be used for estimation of other delay distribution such as the generation interval and serial interval. In both cases, observations are doubly interval censored and a flexible modelling approach using the generalized gamma distribution may be beneficial.

A limitation of our study is that transmission within quarantine facilities cannot be ruled out as some individuals quarantined with infected individuals in one room. However, when transmission within the quarantine facility was observed and mentioned in the public health reports we took this into account in the choice of exposure window: following the loose definition, the end of exposure would in such a case be the moment that an infected room member was transferred to the hospital. This may explain why the estimates with a loose exposure window definition are rather short as individuals may not experience the exponentially growing risk of infection during quarantine. Despite these efforts, some of these transmissions may be unnoticed. Moreover, we did not account for imperfect specificity and sensitivity of the PCR- and rapid antigen tests as this would be challenging, especially as the type of test was mostly unknown. Lastly, one should note that the start of infectiousness may occur earlier than its detection by PCR [Xin, Li, Wu, Li, Lau, Qin, Wang, Cowling, Tsang and Li, 2021].

A fruitful future direction would be to collect data in real-time by using a digital question-

naire form with a scientific purpose besides the typical aim of controlling the outbreak. We have developed a questionnaire form which is openly available via `https://github.com/manhnguy/Contact-Tracing-for-Respiratory-Transmitted-Diseases`. Answers to the questionnaire form can be directed imported into R, and we provide guidance to do so.

In this paper, we provide an estimate of the latency time for the SARS-CoV-2 Delta variant, making novel, realistic assumptions regarding exposure information, and we make our code openly available. To facilitate future estimation of such quantities in a timely manner, more research is needed into both data collection and model assumptions regarding exposure information that match the unruly reality of the infectious disease context.

Acknowledgements

The authors thank Jordache Ramjith for providing his code and Le Van Tan for input on SARS-CoV-2 testing and vaccination practices.

4.7 Supplementary material

4.7.1 Generalized gamma distribution

The probability density function of the generalized gamma distribution as proposed by Stacy and Mihram [1965] is

$$f(t|\theta,\kappa,\delta) = \frac{\frac{\delta}{\theta^{\kappa}}}{\Gamma(\frac{\kappa}{\delta})} t^{\kappa-1} e^{-(\frac{t}{\theta})^{\delta}} \tag{4.4}$$

where θ, κ, $\delta > 0$. The generalized gamma distribution contains the gamma distribution ($\delta = 1$), lognormal ($\frac{\kappa}{\delta} \to \infty$) and Weibull ($\kappa = \delta$) distribution as special cases. The mean is

$$\theta \frac{\Gamma(\frac{\kappa+1}{\delta})}{\Gamma(\frac{\kappa}{\delta})} \tag{4.5}$$

and the variance

$$\theta^2 \left(\frac{\Gamma(\frac{\kappa+2}{\delta})}{\Gamma(\frac{\kappa}{\delta})} - \left(\frac{\Gamma(\frac{\kappa+1}{\delta})}{\Gamma(\frac{\kappa}{\delta})} \right)^2 \right). \tag{4.6}$$

Table 4.1 shows how this parameterization relates to the software implementations of the generalized gamma distribution in the `R` package `flexsurv` [Jackson, 2016] and

in `JAGS` [Plummer, 2017]. We also show the relation between the generalized gamma distribution and the gamma and Weibull distributions in base `R` `dgamma` and `dweibull` distributions, respectively.

For the frequentist approach that we describe in Supplement 4.7.5, we used the relationship between the cumulative distribution functions of the gamma distribution with scale θ and shape κ ($G(t|\theta,\kappa)$) and the generalized gamma distribution ($F(t|\theta,\kappa,\delta)$) [Rubio, 2020], i.e.

$$F(t|\theta,\kappa,\delta) = G(t^{\delta}|\theta^{\delta},\frac{\kappa}{\delta}), \tag{4.7}$$

and the `R` functions provided by Rubio on his webpage.

Table 4.1: Software implementations of generalized gamma distribution as parameterized by Stacy and Mihram [1965] and gamma and Weibull distributions as special cases.

Parameter	**`flexsurv`**	**JAGS, `rjags`**	**base `R`**	
Stacy and Mihram [1965]	`GenGamma.orig(shape, scale, k)`	`dgen.gamma(a, b, c)`	`dgamma(shape, scale)`	`dweibull(shape, scale)`
θ	`scale`	$\frac{1}{b}$	`scale`	`scale`
κ	`shape` $\cdot$ `k`	$a \cdot c$	`shape`	`shape`
δ	`shape`	c	1	`shape`

4.7.2 Parameter estimates of latency time distribution

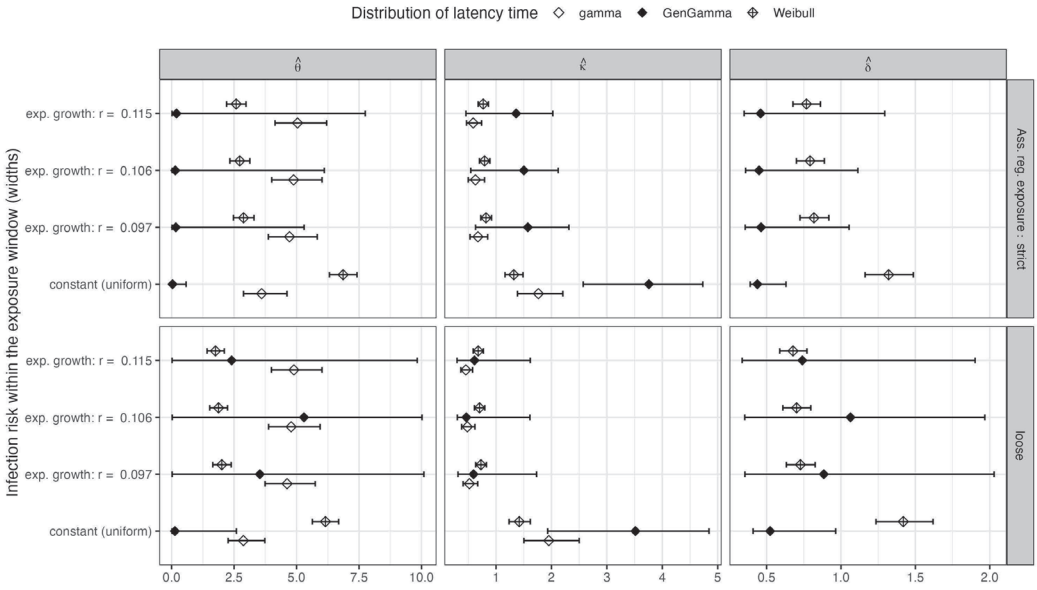

Figure 4.7: Parameter estimates of the latency time distribution for SARS-CoV-2. Parameters refer to the generalized gamma distribution with three parameters θ, κ and δ (columns) [Stacy and Mihram, 1965], of which the gamma (δ = 1, omitted) and Weibull ($\kappa = \theta$) distribution are special cases. Parameter estimates are presented as symbols that refer to the assumed parametric shape of the distribution of latency time and their corresponding 95% credible intervals are represented by error bars. Estimates are given making two different assumptions for the risk of infection within the exposure window (within panel) and two different assumptions regarding the exposure window bounds (rows).

Although the uncertainty in the estimated percentiles based on the generalized gamma distribution is comparable to the gamma and Weibull distributions, the uncertainty in the parameter estimates is considerable (Figure 4.7). This is probably due to strong collinearity between the parameters that define the generalized gamma distribution (Figure 4.8).

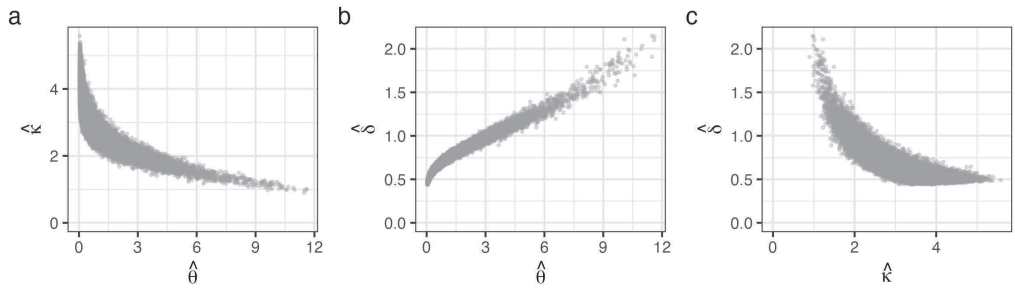

Figure 4.8: Bivariate posterior distribution of parameter pairs of the generalized gamma distribution for the latency time. Settings: handling a strict assumption regarding exposure window and assuming a constant infection risk. Each dot represents one iteration (45 000 in total). Each of the panels (**a**-**c**) visualizes a different combination of parameters. We observe strong collinearity between each of the parameters.

4.7.3 Sensitivity analyses

Figure 6.1 presents the latency time estimates corresponding to sensitivity analyses regarding the observations that were included, whether or not truncation was addressed and the assumption that was made when determining the exposure window bounds. Note that the difference between assuming exponential growth or a constant risk of infection disappears when analysis is restricted to observations with narrow exposure windows (≤ 4 days). The latter estimates are in-between the estimates for the two assumptions regarding the infection risk when all observations are included for analysis.

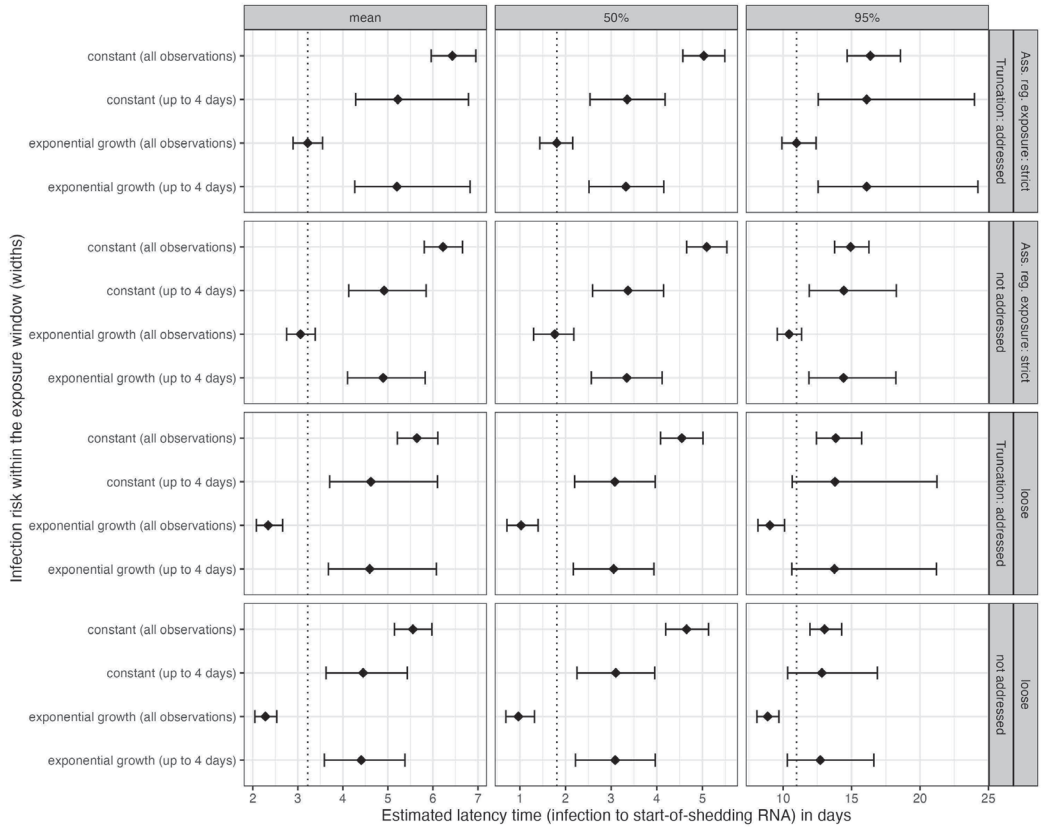

Figure 4.9: Estimated mean and percentiles for different assumptions regarding exposure and right truncation. The y-axis represents the assumed infection risk within the exposure window (r = 0.106 for exponential growth) and whether all observations or observations with narrow ($\leq$ 4 days) were selected for analysis. Panels correspond to the assumption regarding the exposure window bounds and whether truncation was addressed in the analysis or not (rows) and the estimated outcome measure (columns). All analyses assumed a generalized gamma distribution.

4.7.4 Implementation of our model in JAGS

The implementation is surprisingly concise, thanks to the incorporation of both interval censoring and truncation in the JAGS program. The code for a model assuming an increasing risk of infection within the exposure window and a generalized gamma- distributed latency time distribution is:

```
model {
  for(i in 1:N){
```

Table 4.2: Estimates for different assumptions regarding the analysis. All models assume that the latency time distribution follows the shape of generalized gamma. *Abbreviations* Exp. window: (assumption regarding) exposure window. Narrow exp.w.: observations with an exposure window width $\leq$ 4 days. CrI: credible interval.

Truncation	Exp. window	Inf. Risk	Data	Mean	(95% CrI)	50%	(95% CrI)	95%	(95% CrI)	$\hat{\theta}$	(95% CrI)	$\hat{\kappa}$	(95% CrI)	$\hat{\delta}$	(95% CrI)
not addressed	loose	constant (uniform)	all	5.56	(5.15; 5.98)	4.65	(4.19; 5.13)	13.03	(11.96; 14.28)	0.84	(0.07; 7.24)	2.83	(1.33; 4.45)	0.73	(0.5; 1.66)
			narrow exp.w.	4.45	(3.63; 5.43)	3.10	(2.25; 3.95)	12.83	(10.33; 16.88)	0.04	(0.01; 10.17)	2.60	(0.67; 3.93)	0.42	(0.35; 2.00)
		exp. growth: r = 0.097	all	2.36	(2.12; 2.62)	1.05	(0.76; 1.42)	9.02	(8.23; 9.85)	7.74	(2.76; 10.8)	0.39	(0.29; 0.70)	1.49	(0.84; 2.35)
			narrow exp.w.	4.41	(3.59; 5.38)	3.09	(2.21; 3.97)	12.71	(10.31; 16.65)	0.09	(0.02; 12.83)	2.28	(0.52; 3.68)	0.46	(0.37; 3.06)
		exp. growth: r = 0.106	all	2.28	(2.05; 2.53)	0.97	(0.69; 1.32)	8.87	(8.09; 9.69)	7.66	(2.18; 10.63)	0.38	(0.29; 0.72)	1.46	(0.77; 2.26)
			narrow exp.w.	4.41	(3.59; 5.38)	3.09	(2.22; 3.97)	12.71	(10.31; 16.63)	0.12	(0.02; 12.71)	2.23	(0.53; 3.62)	0.47	(0.37; 3.00)
		exp. growth: r = 0.115	all	2.20	(1.98; 2.45)	0.88	(0.64; 1.20)	8.75	(7.97; 9.56)	7.74	(2.87; 10.53)	0.36	(0.28; 0.62)	1.46	(0.83; 2.21)
			narrow exp.w.	4.39	(3.56; 5.35)	3.09	(2.18; 3.99)	12.64	(10.31; 16.44)	0.31	(0.02; 13.64)	1.96	(0.48; 3.51)	0.54	(0.37; 3.54)
	strict	constant (uniform)	all	6.22	(5.81; 6.66)	5.09	(4.65; 5.54)	14.93	(13.76; 16.27)	0.15	(0.02; 1.24)	3.72	(2.49; 4.84)	0.53	(0.43; 0.77)
			narrow exp.w.	4.92	(4.13; 5.85)	3.37	(2.59; 4.15)	14.43	(11.91; 18.27)	0.05	(0.02; 1.50)	2.49	(1.39; 3.55)	0.42	(0.36; 0.71)
		exp. growth: r = 0.097	all	3.21	(2.88; 3.55)	1.98	(1.48; 2.38)	10.49	(9.63; 11.43)	1.60	(0.02; 9.27)	1.08	(0.44; 2.51)	0.72	(0.38; 1.62)
			narrow exp.w.	4.89	(4.11; 5.81)	3.34	(2.57; 4.12)	14.41	(11.91; 18.17)	0.07	(0.02; 2.51)	2.38	(1.21; 3.39)	0.44	(0.37; 0.81)
		exp. growth: r = 0.106	all	3.06	(2.75; 3.39)	1.76	(1.30; 2.18)	10.43	(9.57; 11.35)	4.05	(0.09; 9.96)	0.72	(0.40; 1.92)	0.96	(0.44; 1.72)
			narrow exp.w.	4.89	(4.1; 5.83)	3.34	(2.57; 4.12)	14.41	(11.89; 18.24)	0.05	(0.01; 2.17)	2.47	(1.26; 3.54)	0.42	(0.36; 0.77)
		exp. growth: r = 0.115	all	2.93	(2.64; 3.24)	1.58	(1.15; 2.01)	10.37	(9.52; 11.28)	5.76	(0.17; 10.52)	0.57	(0.36; 1.61)	1.12	(0.47; 1.82)
			narrow exp.w.	4.89	(4.1; 5.81)	3.34	(2.56; 4.11)	14.41	(11.9; 18.20)	0.07	(0.02; 2.27)	2.38	(1.24; 3.41)	0.44	(0.36; 0.78)
addressed	loose	constant (uniform)	all	5.64	(5.21; 6.11)	4.55	(4.08; 5.01)	13.84	(12.43; 15.73)	0.13	(0.02; 2.59)	3.51	(1.93; 4.84)	0.52	(0.41; 0.96)
			narrow exp.w.	4.62	(3.71; 6.10)	3.08	(2.20; 3.96)	13.79	(10.67; 21.24)	0.05	(0.02; 7.26)	2.31	(0.83; 3.58)	0.42	(0.34; 1.40)
		exp. growth: r = 0.097	all	2.44	(2.16; 2.77)	1.16	(0.80; 1.52)	9.15	(8.25; 10.25)	3.53	(0.02; 10.09)	0.59	(0.31; 1.73)	0.88	(0.35; 2.03)
			narrow exp.w.	4.59	(3.67; 6.06)	3.06	(2.18; 3.95)	13.7	(10.61; 21.03)	0.06	(0.02; 10.64)	2.20	(0.64; 3.53)	0.43	(0.34; 2.13)
		exp. growth: r = 0.106	all	2.34	(2.08; 2.66)	1.03	(0.72; 1.40)	9.03	(8.16; 10.10)	5.30	(0.03; 10.02)	0.46	(0.30; 1.61)	1.06	(0.35; 1.97)
			narrow exp.w.	4.60	(3.68; 6.08)	3.05	(2.17; 3.94)	13.75	(10.64; 21.20)	0.05	(0.02; 8.76)	2.24	(0.73; 3.53)	0.42	(0.34; 1.65)
		exp. growth: r = 0.115	all	2.30	(2.03; 2.63)	0.98	(0.67; 1.32)	8.94	(8.03; 10.20)	2.40	(0.02; 9.83)	0.61	(0.30; 1.62)	0.74	(0.34; 1.90)
			narrow exp.w.	4.59	(3.67; 6.04)	3.06	(2.18; 3.94)	13.68	(10.61; 20.98)	0.06	(0.02; 10.41)	2.19	(0.65; 3.51)	0.43	(0.34; 2.04)
	strict	constant (uniform)	all	6.43	(5.96; 6.95)	5.03	(4.57; 5.49)	16.37	(14.68; 18.57)	0.04	(0.01; 0.58)	3.76	(2.57; 4.73)	0.44	(0.39; 0.63)
			narrow exp.w.	5.22	(4.28; 6.79)	3.35	(2.54; 4.18)	16.10	(12.56; 23.98)	0.05	(0.01; 1.17)	2.21	(1.28; 3.26)	0.4	(0.33; 0.64)
		exp. growth: r = 0.097	all	3.32	(3.00; 3.65)	1.94	(1.57; 2.30)	11.07	(10.02; 12.45)	0.17	(0.02; 5.30)	1.57	(0.63; 2.31)	0.46	(0.36; 1.05)
			narrow exp.w.	5.20	(4.26; 6.79)	3.32	(2.51; 4.16)	16.11	(12.56; 24.05)	0.05	(0.01; 1.22)	2.20	(1.25; 3.25)	0.4	(0.33; 0.65)
		exp. growth: r = 0.106	all	3.22	(2.89; 3.55)	1.81	(1.44; 2.16)	10.98	(9.91; 12.41)	0.15	(0.02; 6.11)	1.50	(0.54; 2.12)	0.45	(0.36; 1.11)
			narrow exp.w.	5.20	(4.26; 6.82)	3.32	(2.51; 4.15)	16.10	(12.55; 24.23)	0.05	(0.02; 1.02)	2.21	(1.30; 3.24)	0.4	(0.33; 0.62)
		exp. growth: r = 0.115	all	3.11	(2.78; 3.45)	1.67	(1.30; 2.03)	10.88	(9.81; 12.35)	0.20	(0.02; 7.75)	1.36	(0.46; 2.02)	0.46	(0.35; 1.29)
			narrow exp.w.	5.20	(4.26; 6.80)	3.32	(2.51; 4.15)	16.09	(12.54; 24.12)	0.05	(0.01; 1.35)	2.22	(1.24; 3.27)	0.4	(0.33; 0.66)

```
# Interval censoring of the endpoint
          type_R[i] ~ dinterval( Y[i] , C[i, 1:2] )
           C[i,1] <- max( 0.000000001, (R0[i] - L[i]) )
           C[i,2] <- max( 0.000000001, (R1[i] - L[i]) )

# Exponential growth (or decay)
           L_star[i] ~ dexp(r) T(0, L1[i])
           L[i] <- L1[i] - L_star[i]

# Generalized gamma-distributed time-to-event
           Y[i] ~ dgen.gamma(a, b, c)
  }

# Priors
  a ~ dnorm(0, 1/1000)I(0, )
  b ~ dnorm(0, 1/1000)I(0, )
  c ~ dnorm(0, 1/1000)I(0, )
  r ~ dnorm(r_est, prec_r)
  prec_r <- 1/(r_se^2)
}
```

The interval censoring of the endpoint is incorporated by the JAGS function `dinterval`. The interval censoring of the origin is implemented via truncation on the exposure window `T(0, L1[i])` of the pre-specified distribution (here exponential `dexp(r)`). Exponential decay can be implemented easily by replacing `L_star` directly by `L[i]`, saving one line. The parameterization of the generalized gamma distribution in JAGS differs from the one proposed by Stacy and Mihram [1965]. In our R code we rewrite the parameter estimates accordingly, see Table 4.1. To avoid any confusion, in the above code we use a, b, and c. We use an uninformative truncated normal prior for these parameters, via the term $I(0,)$. For the exponential growth factor r, we assume a normal distribution parameterized according to the input data, i.e. the estimate (`r_est`) and its Standard Error (`r_se`). Note that JAGS works with precision rather than standard deviation.

We verified the validity of this implementation of right truncated data by means of a small simulation study of 500 generated data sets per scenario and 1000 infected individuals per data set, before truncation. We generated data assuming a random exposure window width varying from one to five days and a constant risk of infection within the window. We chose a gamma distributed latency time as estimated by Xin *et al.* [2021] (shape = 4.05, rate = 0.74; median 5.03; 95^{th} percentile 10.57). The endpoint was observed up to the day accurate. Quarantine started at the end of the exposure window. Individuals were tested at the end of quarantine. We mimicked three scenarios with respect to truncation due to end of quarantine: i) individuals left quarantine 5, 10, 15, 20 or 25 days after entering, each occurring with equal probability; ii) quarantine lasted 7 days for all; iii) quarantine lasted 7 or 14 days (with equal probability). Only those individuals that tested positive before exiting quarantine were included for the analyses, meaning that those individuals for whom start-of-infectiousness occurred later remained unobserved. Our simulation code can be accessed via the example section the R help file for function `Estimate_doublIn` in our R package `doublIn`.

Figure 4.10 shows that our JAGS code adequately addresses truncation. Note that the difference between the analyses with and without correction for truncation is small when the level of truncation is very mild (14 or 21 days) whereas the difference is large when the level of truncation varies (5, 10, 15, 20, or 25 days) or is consistently strong (7 days). The coverage when truncation is not addressed is especially poor for the tail percentile. For quarantine scenario ii), 150 of 500 data sets did not provide a model fit

for one of the two models (addressing truncated or naive) which we hypothesize was due to too little information in the data set.

4.7.5 Alternative analyses

We explored several alternative analyses, that were eventually not suitable for our data, but may inspire the reader facing another data set.

We explored an equivalent frequentist approach, where we built upon `R` code by Ramjith *et al.* [2022] suitable for doubly interval censored observations with two non-overlapping or completely overlapping windows. We utilized the idea present in the source code of the `R` package `coarseDataTools` on representing the observation when exposure and start-of-shedding windows partially overlap and adapted the code by Ramjith *et al.* accordingly. Then, the contribution to the likelihood can be written as the sum of three district parts as shown in Figure 4.11. The same expressions are used as in the main text, e.g. Expression 4.2 for type (a) and 4.1 for type (b) and (c), but the start and end of the windows containing the origin (E) and (S) are adapted to match the respective part. With our data set we faced convergence issues that we hypothesize to be related to local maxima in the likelihood.

In an attempt to move away from the assumption of a constant risk of infection, we considered exponential risk as described in the main text but also two other variations. In both we first estimated the risk of infection over calendar time using the nonparametric maximum likelihood estimator for interval censored data (NPMLE; `R` package `interval` [Fay and Shaw, 2010]). In the first variation we considered a piecewise constant infection risk where we assume a constant risk during each day to which the NPMLE, a discrete estimator, assigned probability mass. In the second variation, we determined one or multiple peaks and lows in the risk of infection with the function `find_peaks(span = 3, ignore_treshold = 0.1)` from R package `ggpmisc` [Aphalo, 2023; Dayal, 2021]. For each of the decreasing and increasing phases, we estimated the corresponding exponential growth factor using the R package `incidence` [Kamvar et al., 2019]. In the analysis, we used the 'individual' exponential growth factor that was applicable midway the individual's exposure window. However, we saw that the NPMLE had a very limited amount of jumps, indicating that our data contained too much uncertainty regarding the moment of infection to choose one of these approaches.

We also fitted the infection risk distribution within each of the three largest clusters. Again, we saw that this gave too little information in order to provide a finescaled NPMLE.

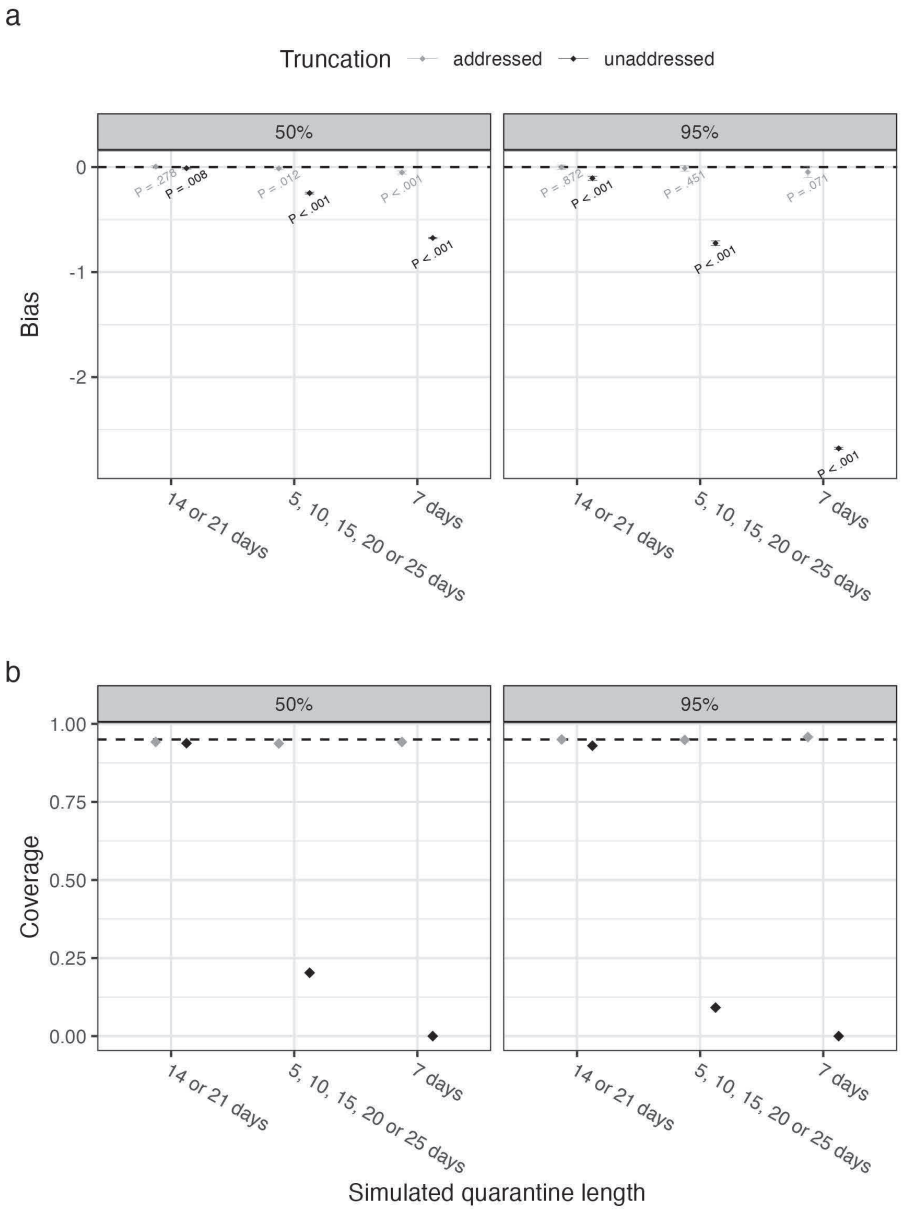

Figure 4.10: Simulation results to verify our JAGS implementation. Colors represent whether or not truncation was addressed in the analysis. Figure (**a**) visualizes the bias, its 95% Confidence Interval and the corresponding P-value (t-test). Figure (**b**) presents the coverage proportion of the true quantiles by the Confidence Intervals.

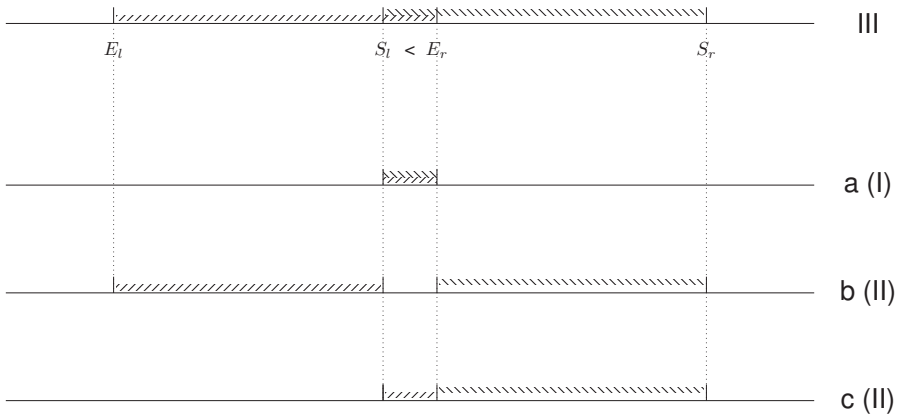

Figure 4.11: Illustration of data representation of partially overlapping exposure and start-of-shedding windows. In our code for the frequentist approach, we decompose partially overlapping windows (type III in Figure 4.2) in three distinct parts, one for the completely overlapping part (a) or two for the non-overlapping parts to the left and right (b and c). Part a is conform type I in Figure 4.2, whereas part b and c are conform type II. Inspired by the source code in the `coarseDataTools` package [Reich et al., 2009], we use this idea to write the likelihood of an observation with partially overlapping windows, by summing the likelihoods of part a, b and c.